Research Article | Vol. 25, No. 22 | 30 Oct 2017 | OPTICS EXPRESS 27785
Optics EXPRESS

Optical receiver sensitivity enhancement by single- and dual-band fiber optical parametric amplifier

JIQIANG KANG,[1] M. E. MARHIC,[2] BOWEN LI,[1] SISI TAN,[1] XIE WANG,[1] AND KENNETH K. Y. WONG[1,*]

[1]*Department of Electrical and Electronic Engineering, The University of Hong Kong, Pokfulam Road, Hong Kong SAR, China*
[2]*Deceased August 2014*
**kywong@eee.hku.hk*

Abstract: A semi-classical model is proposed theoretically and demonstrated experimentally on the optical receiver sensitivity enhancement by single-band (signal or idler) and dual-band (signal and idler) fiber optical parametric amplifier (FOPA). The sensitivity enhancement by single-band is determined by the gain of FOPA and the transmission loss of signal and idler, and it can be further improved by up to 3-dB using amplified signal and phase-conjugated idler together at dual-band configuration. The theoretical results are experimentally verified in both fiber communication and biomedical imaging applications. This detection sensitivity enhancement scheme can be potentially applied in the scenarios where ultrafast broadband signal at low-power level is being handled.

OCIS codes: (060.2320) Fiber optics amplifiers and oscillators; (190.4380) Nonlinear optics, four-wave mixing; (190.4410) Nonlinear optics, parametric processes; (060.7140) Ultrafast processes in fibers.

References and links

1. S. Cova, M. Ghioni, A. Lacaita, C. Samori, and F. Zappa, "Avalanche photodiodes and quenching circuits for single-photon detection," Appl. Opt. **35**(12), 1956–1976 (1996).
2. M. Stipcević, "Active quenching circuit for single-photon detection with Geiger mode avalanche photodiodes," Appl. Opt. **48**(9), 1705–1714 (2009).
3. J. Zhang, M. A. Itzler, H. Zbinden, and J. Pan, "Advances in InGaAs/InP single-photon detector systems for quantum communication," Light Sci. Appl. **4**, e286 (2015).
4. G. P. Agrawal, *Fiber-Optic Communication Systems* (John Wiley & Sons, 2002), Chap. 4.
5. K. Mochizuki, Y. Namihira, M. Kuwazuru, and M. Nunokawa, "Influence of hydrogen on optical fiber loss in submarine cables," J. Lightwave Technol. **2**(6), 802–807 (1984).
6. S. A. Filatova, I. A. Shcherbakov, and V. B. Tsvetkov, "Optical properties of animal tissues in the wavelength range from 350 to 2600 nm," J. Biomed. Opt. **22**(3), 35009 (2017).
7. G. P. Agrawal, *Nonlinear Fiber Optics* (Academic, 2007).
8. American National Standards Institute, "American national standard for safe use of lasers," ANSI Z136.1–200 (ANSI, 2000).
9. G. Konstantatos and E. H. Sargent, "Nanostructured materials for photon detection," Nat. Nanotechnol. **5**(6), 391–400 (2010).
10. R. Kumar, E. Barrios, A. MacRae, E. Cairns, E. H. Huntington, and A. I. Lvovsky, "Versatile wideband balanced detector for quantum optical homodyne tomography," Opt. Commun. **285**(24), 5259–5267 (2012).
11. Y. Painchaud, M. Poulin, M. Morin, and M. Têtu, "Performance of balanced detection in a coherent receiver," Opt. Express **17**(5), 3659–3672 (2009).
12. H. Hansen, T. Aichele, C. Hettich, P. Lodahl, A. I. Lvovsky, J. Mlynek, and S. Schiller, "Ultrasensitive pulsed, balanced homodyne detector: application to time-domain quantum measurements," Opt. Lett. **26**(21), 1714–1716 (2001).
13. Keysight Technologies, "Preamplifiers and System Noise Figure," *http://literature.cdn.keysight.com/litweb/pdf/5989-5742EN.pdf*.
14. Y. Yamamoto and H. Tsuchiya, "Optical receiver sensitivity improvement by a semiconductor laser preamplifier," Electron. Lett. **16**(6), 233–235 (1980).
15. B. Mikkelsen, C. G. Jorgensen, N. Jensen, T. Durhuus, K. E. Stubkjaer, P. Doussiere, and B. Fernier, "High-Performance Semiconductor Optical Preamplifier Receiver at 10 Gb/s," IEEE Photonics Technol. Lett. **5**(9), 1096–1097 (1993).

#303588 https://doi.org/10.1364/OE.25.027785
Journal © 2017 Received 31 Jul 2017; revised 19 Oct 2017; accepted 22 Oct 2017; published 26 Oct 2017

Optics EXPRESS

16. T. Saito, Y. Sunohara, K. Fukagai, S. Ishikawa, N. Henmi, S. Fujita, and Y. Aoki, "High receiver sensitivity at 10 Gb/s using an Er-doped fiber preamplifier pumped with a 0.98 mu m laser diode," IEEE Photonics Technol. Lett. **3**(6), 551–553 (1991).
17. M. S. Salisbury, P. F. McManamon, and B. D. Duncan, "Sensitivity improvement of a 1-um ladar system incorporating an optical fiber preamplifier," Opt. Eng. **32**(11), 2671–2680 (1993).
18. B. P. P. Kuo, K. Shimizu, P. C. Chui, and K. K. Y. Wong, "Receiver sensitivity improvement for ON-OFF keying signal by using optical parametric amplifier and balanced detection,"in *Proceedings of the IEEE/LEOS Winter Topical Meeting Series,* (IEEE, 2008), pp. 59–60.
19. Y. Liang, J. Li, P. C. Chui, and K. K. Y. Wong, "High-sensitivity optical preamplifier for WDM systems using an optical parametric amplifier," IEEE Photonics Technol. Lett. **21**(20), 1562–1564 (2009).
20. M. E. Marhic, *Fiber Optical Parametric Amplifiers, Oscillators and Related Devices* (Cambridge University Press, 2012).
21. M. E. Marhic, P. A. Andrekson, P. Petropoulos, S. Radic, C. Peucheret, and M. Jazayerifar, "Fiber optical parametric amplifiers in optical communication systems," Laser Photonics Rev. **9**(1), 50–74 (2015).
22. K. Goda, K. K. Tsia, and B. Jalali, "Serial time-encoded amplified imaging for real-time observation of fast dynamic phenomena," Nature **458**(7242), 1145–1149 (2009).
23. K. K. Tsia, K. Goda, D. Capewell, and B. Jalali, "Performance of serial time-encoded amplified microscope," Opt. Express **18**(10), 10016–10028 (2010).
24. X. Wei, A. K. S. Lau, Y. Xu, C. Zhang, A. Mussot, A. Kudlinski, K. K. Tsia, and K. K. Y. Wong, "Broadband fiber-optical parametric amplification for ultrafast time-stretch imaging at 1.0 μm," Opt. Lett. **39**(20), 5989–5992 (2014).
25. M. E. Marhic, K. K. Y. Wong, and L. G. Kazovsky, "Wide-band tuning of the gain spectra of one-pump fiber optical parametric amplifiers," IEEE J. Sel. Top. Quantum Electron. **10**(5), 1133–1141 (2004).
26. T. Torounidis, P. A. Andrekson, and B. A. Olsson, "Fiber-optical parametric amplifier with 70-dB gain," IEEE Photonics Technol. Lett. **18**(10), 1194–1196 (2006).
27. S. D. Jackson, "Towards high-power mid-infrared emission from a fibre laser," Nat. Photonics **6**, 423–431 (2012).
28. T. Torounidis, H. Sunnerud, P. O. Hedekvist, and P. A. Andrekson, "Amplification of WDM signals in fiber-based optical parametric amplifiers," IEEE Photonics Technol. Lett. **15**(8), 1061–1063 (2003).
29. K. K. Y. Wong, G. W. Lu, and L. K. Chen, "Polarization-interleaved WDM signals in a fiber optical parametric amplifier with orthogonal pumps," Opt. Express **15**(1), 56–61 (2007).
30. J. Kang, X. Wei, B. Li, X. Wang, L. Yu, S. Tan, C. Jinata, and K. K. Y. Wong, "Sensitivity enhancement in swept-source optical coherence tomography by parametric balanced detector and amplifier," Biomed. Opt. Express **7**(4), 1294–1304 (2016).
31. C. McKinstrie, M. Yu, M. G. Raymer, and S. Radic, "Quantum noise properties of parametric processes," Opt. Express **13**(13), 4986–5012 (2005).
32. C. J. S. de Matos, D. A. Chestnut, P. C. Reeves-Hall, and J. R. Taylor, "Continuous-wave-pumped Raman-assisted fiber optical parametric amplifier and wavelength converter in conventional dispersion-shifted fiber," Opt. Lett. **26**(20), 1583–1585 (2001).
33. M. N. Islam and O. Boyraz, "Fiber parametric amplifiers for wavelength band conversion," IEEE J. Sel. Top. Quantum Electron. **8**(3), 527–537 (2002).
34. H. Hu, R. M. Jopson, A. H. Gnauck, S. Randel, and S. Chandrasekhar, "Fiber nonlinearity mitigation of WDM-PDM QPSK/16-QAM signals using fiber-optic parametric amplifiers based multiple optical phase conjugations," Opt. Express **25**(3), 1618–1628 (2017).
35. A. Kumpera, R. Malik, A. Lorences-Riesgo, and P. A. Andrekson, "Parametric coherent receiver," Opt. Express **23**(10), 12952–12964 (2015).
36. J. L. Blows and S. E. French, "Low-noise-figure optical parametric amplifier with a continuous-wave frequency-modulated pump," Opt. Lett. **27**(7), 491–493 (2002).
37. P. Kylemark, P. O. Hedekvist, H. Sunnerud, M. Karlsson, and P. A. Andrekson, "Noise characteristics of fiber optical parametric amplifiers," J. Lightwave Technol. **22**(2), 409–416 (2004).
38. A. Durécu-Legrand, C. Simonneau, D. Bayart, A. Mussot, T. Sylvestre, E. Lantz, and H. Maillotte, "Impact of pump OSNR on noise figure for fiber optical parametric amplifiers," IEEE Photonics Technol. Lett. **17**(6), 1178–1180 (2005).
39. P. Kylemark, M. Karlsson, and P. A. Andrekson, "Gain and wavelength dependence of the noise-figure in fiber optical parametric amplifiers," IEEE Photonics Technol. Lett. **18**(11), 1255–1257 (2006).
40. A. Bogris, D. Syvridis, P. Kylemark, and P. A. Andrekson, "Noise characteristics of dual-pump fiber-optic parametric amplifiers," J. Lightwave Technol. **23**(9), 2788–2795 (2005).
41. P. L. Voss and P. Kumar, "Raman-noise-induced noise-figure limit for $\chi^{(3)}$ parametric amplifiers," Opt. Lett. **29**(5), 445–447 (2004).
42. R. Tang, P. L. Voss, J. Lasri, P. Devgan, and P. Kumar, "Noise-figure limit of fiber-optical parametric amplifiers and wavelength converters: experimental investigation," Opt. Lett. **29**(20), 2372–2374 (2004).
43. S. M. M. Friis, K. Rottwitt, and C. J. McKinstrie, "Raman and loss induced quantum noise in depleted fiber optical parametric amplifiers," Opt. Express **21**(24), 29320–29331 (2013).
44. Z. Tong, A. Bogris, M. Karlsson, and P. A. Andrekson, "Full characterization of the signal and idler noise figure spectra in single-pumped fiber optical parametric amplifiers," Opt. Express **18**(3), 2884–2893 (2010).

Optics EXPRESS

45. N. A. Olsson, "Lightwave systems with optical amplifiers," J. Lightwave Technol. **7**(7), 1071–1082 (1989).
46. R. Huber, M. Wojtkowski, K. Taira, J. Fujimoto, and K. Hsu, "Amplified, frequency swept lasers for frequency domain reflectometry and OCT imaging: design and scaling principles," Opt. Express **13**(9), 3513–3528 (2005).

1. Introduction

Optical receiver is a key part in a variety of light wave systems, such as optical communication system, and optical bio-medical imaging modality, etc. The function of a typical optical receiver is to transform signal from the optical domain to the electrical domain. Optical receiver normally consists of a photoelectric conversion part, i.e. the sensor, and a complicated electrical circuit to process the converted signal [1–3]. Among all the parameters that describe the performance of an optical receiver, receiver sensitivity is a crucial factor that represents the minimum optical power required for the receiver to achieve a sufficient signal-to-noise ratio (SNR) [4]. Therefore, when a system is constructed with a certain receiver, system's minimum optical-power requirement (detection sensitivity) can be identified according to the receiver sensitivity. In many systems, the optical power will be significantly attenuated before reaching the receiver. For example, there is inevitable loss along optical transmission fiber and components in long-haul optical communication systems [5]. Similarly, highly scattering and absorbing bio-tissues attenuate optical signals in optical bio-medical imaging systems [6]. Consequently, very large initial optical power may be required at the input of these system in order to meet the requirement of the receiver sensitivity. However, the requirement of high optical input power brings additional issues for many applications. For example, in optical fiber communication systems, large power will induce undesired fiber nonlinear effects, which distorts the transmitted pulse and subsequently increases bit-error rate (BER) [7]. Moreover, in optical bio-medical imaging system, large illumination power on the bio-sample will induce photo-damage, photo-bleaching, and photo-toxicity to the bio-samples [8]. Therefore, in such systems where high optical input power needs to be avoided, the enhancement of optical receiver sensitivity become critically important.

Several techniques have been proposed and demonstrated for this goal, such as implementing a more sensitive sensor using novel materials together with a more precise detecting circuit to post-process weak electrical signal with good noise suppression [9]. Besides, by setting two identical sensors to work in a balanced topology, a balanced detector (BD) can be realized to suppress the common-mode noise and thus increase the detection SNR and the dynamic range [10–12]. These two schemes have successfully promoted the development of highly sensitive optical receivers. However, even higher detection sensitivity can be achieved for a fixed receiver using pre-amplification. Quite similar scenario is encountered in microwave system, where a broadband low-noise preamplifier is always set close to the antenna side to enhance the sensitivity as well as the dynamic range, thus compensating the degradation from the attenuation [13]. The detection sensitivity enhancement scheme with external preamplifier does not modify the receiver sensitivity, but it helps achieve the same performance with much lower system input power.

In lightwave system, different kinds of optical pre-amplifiers can be adopted for the enhancement of detection sensitivity, such as semiconductor amplifier [14,15], erbium-doped fiber amplifier [16,17], and fiber optical parametric amplifier (FOPA) [18,19], etc. Among all of those schemes, FOPA exhibits remarkable advantages comparing with the others in terms of response time, optical spectral range, and gain value. First of all, FOPA has ultrafast response time at femtoseconds (fs) level that makes it a good candidate in ultrafast signal amplification [20], such as in terabit transmission system [21] and ultrafast spectrally encoded time-stretch microscope [22–24]. Furthermore, FOPA provides much broader gain bandwidth and larger gain. 400-nm gain bandwidth and 70 dB gain have been reported [25,26], while typical gain bandwidth for gain fiber or semiconductor amplifier are less than 100 nm with less than 40 dB gain value [27]. These features make FOPA a very good solution for broadband small signal amplification, such as in long-haul wavelength-division multiplexing

Optics EXPRESS

(WDM) system [28,29] and swept-source optical coherence tomography (SS-OCT) [30]. Besides, there is a unique characteristic that distinguishes FOPA from other amplifiers, i.e. FOPA not only amplifies the input signal like a typical amplifier but it also generates a phase-conjugated idler [31]. The generated idler has the same time domain waveform profile with the amplified signal but locates at different wavelength range. This feature has been widely explored for broadband wavelength conversion and signal multicasting [32,33]. Recently, polarization-insensitive FOPA has been successfully used to amplify 1.024-Tbit/s WDM polarization-division multiplexed (PDM) quaternary phase-shift keying (QPSK) signal and 2.048-Tbit/s WDM PDM 16-state quadrature amplitude modulation (16-QAM) signal, and the phase conjugation idler is used to mitigate the fiber nonlinearity [34]. This work, together with many others previous works, verified the capability of the FOPA in handling those advanced modulation formats in next-generation optical communications systems. Normally, signal and idler are used separately in time domain, but sometimes signal and idler are used simultaneously without splitting. For clarity, single-band FOPA is named here when either signal or idler band is used after the FOPA, while dual-band FOPA refers to the cases that both signal and idler bands are used simultaneously.

To investigate the capability of optical receiver sensitivity enhancement using FOPA in practical applications, Liang *et al*. explored both single- and dual-band FOPA in WDM systems with 10-Gb/s return-to-zero on-off keying format WDM system [19]. Wei *et al*. and Kang *et al*. exploited the FOPA-based sensitivity enhancement scheme in a spectrally encoded ultrafast time-stretch microscope at 1.0-μm wavelength window and SS-OCT system at 1.5-μm wavelength regime respectively [24,30]. Those extensive experimental work verified the receiver sensitivity enhancement capability of FOPA either in the optical communication regime or in the optical bio-medical imaging application. Moreover, single-band and dual-band FOPA show different performance according to those experimental work, and the sensitivity enhancement by the dual-band FOPA is about 3-dB higher than the single-band FOPA. Comparing with normally used coherent receiver where a local oscillator (LO) should be provided, the advantage of this sensitivity enhancement scheme is LO free, which makes it a suitable choice at biomedical imaging where a LO is hard to generate. It is worth noting that, when a LO signal can be obtained easily, a type of parametric coherence receiver based on FOPA as was described in Ref [35] is also a suitable implementation for high sensitivity detection in coherent lightwave systems.

Although those extensive experiments successfully verified the effectiveness of sensitivity enhancement by this scheme, the corresponding theory work was largely unreported specifically. To address this knowledge gap and comprehensively study the sensitivity enhancement of using single- and dual-band FOPA, a theoretical analysis based on semi-classical model is elaborated at section 2 in this paper. At section 3, those previous experimental work on receiver sensitivity enhancement by single- and dual-band FOPA covering optical communication and bio-medical imaging are reviewed to provide solid experimental support for the theoretical analysis.

2. Principles of sensitivity enhancement with single- and dual-band FOPA

At this section, we focus on one-pump phase-insensitive FOPA (PI-FOPA) working at non-saturated regime. The schematic diagram of the PI-FOPA based single- and dual-band optical receiver sensitivity enhancement technique is shown in Fig. 1.

Optics EXPRESS

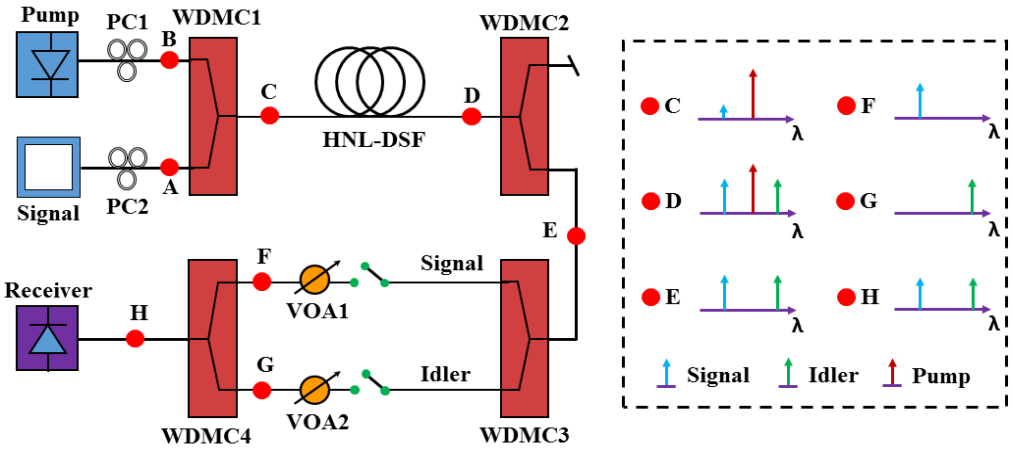

Fig. 1. Schematic of the optical receiver sensitivity enhancement scheme. PC: polarization controller; WDMC: wavelength-division multiplexing coupler; HNL-DSF: highly-nonlinear dispersion-shifted fiber; VOA: variable optical attenuator.

Assuming a single frequency optical signal with angular frequency ω_s is incident at the input (point A), and the pump frequency is ω_p (point B). The pump and signal are combined by a WDM coupler, i.e. WDMC1 at Fig. 1. We assume that a spool of highly-nonlinear dispersion-shifted fiber (HNL-DSF) is used as the gain platform for FOPA, and the FOPA has a signal gain G. In that case, there also appears an idler at frequency $\omega_i = 2\omega_p - \omega_s$ at the FOPA's output (point D), and the idler power at point D is about the same as the amplified signal power. The residual pump also emerges at point D, and it is then removed by a WDM coupler, i.e. WDMC2 in Fig. 1. The signal and idler are then separated by a WDM coupler, i.e. WDMC3 at Fig. 1. To switch between single- and dual-band cases, another C/L band WDM coupler, i.e. WDMC 4 at Fig. 1, is used. WDMC3 and WDMC4 is connected by patchcords and the loss for signal and idler bands are balanced by attenuators. The final output power from WDMC4 is collected by an optical receiver. The optical frequency component at each point is illustrated in the inset dash box at Fig. 1.

For practical one pump PI-FOPA, the residual pump noise [36], pump transferred noise [37–40], Raman phonon seeded noise [41,42], and amplified quantum noise [37,43] are responsible for the SNR degradation of the amplified signal. Among all those noises, the amplified quantum noise is the inherent one for PI-FOPA, and the remaining kinds can be minimized or removed [44], such as by cooling down optical fiber to reduce Raman phonon seeded noise and applying low noise figure (NF) EDFA and good quality filters to control the pump transferred noise and residual pump noise. To reveal the underlying principles of sensitivity enhancement with single- and dual-band FOPA, an ideal PI-FOPA model is used here and only amplified quantum noise is considered while the remaining noises are ignored in the following analysis. The analysis relies on a semi-classical model and the input filed is assumed in a coherent state (CS).

Based on these assumptions, the signal electric field at point A is written as $E_s + e_s$, where E_s is a deterministic signal, and e_s is a random field corresponding to vacuum fluctuations. The idler electric field at A is only due to random vacuum fluctuations, and is denoted by e_i. For an ideal FOPA with 3-dB noise figure, the slowly varying envelopes of the signal and idler fields at D are then approximately the same, and equal to $G^{1/2}(E_s + e_s + e_i)$, respectively at ω_s and ω_i.

The signal and idler paths between A and E respectively have transmittances α and β. Hence the total instantaneous (short-term average) power incident on the receiver is

$$P_A = \alpha G\left|E_s + e_s + e_i\right|^2 + \beta G\left|E_s + e_s + e_i\right|^2 = (\alpha + \beta) G\left|E_s + e_s + e_i\right|^2. \qquad (1)$$

Optics EXPRESS

Let η denote the detector responsivity. Then the total detected current is

$$I = \eta P_A + i_n = \eta(\alpha+\beta)G\left|E_s + e_s + e_i\right|^2 + i_n, \tag{2}$$

where i_n is the dark current at the detector. The mean detector current is then obtained by ensemble averaging, denoted by "< >".

$$\begin{aligned} I_m &= \eta(\alpha+\beta)G\left\langle\left|E_s + e_s + e_i\right|^2\right\rangle + \left\langle i_n\right\rangle = \eta(\alpha+\beta)G\left(\left|E_s\right|^2 + \left\langle\left|e_s\right|^2\right\rangle + \left\langle\left|e_i\right|^2\right\rangle\right) \\ &= \eta(\alpha+\beta)G\left(P_s + 2\tilde{P}_s\right) \end{aligned}, \tag{3}$$

where P_s is the input signal power, and $\tilde{P}_s = \left\langle\left|e_s\right|^2\right\rangle = \left\langle\left|e_i\right|^2\right\rangle$ is the power of the input vacuum fluctuations at either ω_s or ω_i, and i_n has zero means. The output electrical signal proportional to P_s is thus determined by

$$I_{sig} = \eta(\alpha+\beta)GP_s \tag{4}$$

Moreover, the variance of the detector current is

$$\begin{aligned} \delta I^2 &= \left\langle I^2\right\rangle - I_m{}^2 = \left\langle\left[\eta(\alpha+\beta)G\left|E_s + e_s + e_i\right|^2 + i_n\right]^2\right\rangle - \left[\eta(\alpha+\beta)G\left(P_s + 2\tilde{P}_s\right)\right]^2 \\ &\approx 4\eta^2(\alpha+\beta)^2 G^2 P_s\tilde{P}_s + i_n^2 = 4\eta^2(\alpha+\beta)^2 G^2 P_s\tilde{P}_s + \delta i_n{}^2 \end{aligned}. \tag{5}$$

The first term at the final result of Eq. (5) represents the beating signal between amplified quantum noise and amplified signal when they are received by the photodetector, while the second term represents the variance of the dark current noise. To obtain the last form of Eq. (5), the fact that e_s, e_i and i_n are orthogonal random variables with zero means is used. We also neglect terms in e_s and e_i that do not involve E_s, as they are insignificant for a relatively strong CS input.

We can now calculate the electrical output signal to noise ratio (SNR). It is given by

$$SNR_{out} = \left(\frac{I_{sig}}{\delta I}\right)^2 = \frac{\left[\eta(\alpha+\beta)GP_s\right]^2}{4\eta^2(\alpha+\beta)^2 G^2 P_s\tilde{P}_s + \delta i_n{}^2} = \frac{P_s^2}{4P_s\tilde{P}_s + u}. \tag{6}$$

where

$$u = \frac{\delta i_n{}^2}{\left[\eta(\alpha+\beta)G\right]^2}. \tag{7}$$

We can then define the sensitivity $S(\alpha, \beta)$ as the value of P_s (input signal power at A) for which a suitable value of SNR_{out} is obtained. For example, SNR_{out} can be determined by the desired value of the system's BER. Let SNR_0 denote this desired value, we then have the equation from Eq. (6)

$$SNR_0 = \left(\frac{I_{out}}{\delta I}\right)^2 = \frac{\left[\eta(\alpha+\beta)GS(\alpha,\beta)\right]^2}{4\eta^2(\alpha+\beta)^2 G^2 S(\alpha+\beta)\tilde{P}_s + \delta i_n{}^2} = \frac{S(\alpha,\beta)^2}{4\tilde{P}_s S(\alpha,\beta) + u}. \tag{8}$$

Equation (8) can then be solved for $S(\alpha, \beta)$, with the result

$$S(\alpha,\beta) = 2\tilde{P}_s SNR_0\left[1 + \sqrt{1 + \frac{v}{(\alpha+\beta)^2}}\right], \tag{9}$$

where

Optics EXPRESS

$$v = \frac{\delta i_n^{\,2}}{4\tilde{P}_s \eta^2 G^2 SNR_0}. \tag{10}$$

This is the sensitivity requirement for dual-band FOPA.

Consider the situation that if there is no FOPA used, i.e. $G = 1$ at Eq. (10), and no idler is generated as well ($\beta = 0$), and the receiver sensitivity for a target SNR_0 at this case is,

$$S_N(\alpha, 0) = 2\tilde{P}_s SNR_0 \left[1 + \sqrt{1 + \frac{v_N}{\alpha^2}}\right], \tag{11}$$

where

$$v_N = \frac{\delta i_n^{\,2}}{4\tilde{P}_s \eta^2 SNR_0}. \tag{12}$$

If FOPA is switched on but only the amplified signal band is selected after point D, we have G>1 and $\beta = 0$. From Eq. (9), the sensitivity for this case is

$$S(\alpha, 0) = 2\tilde{P}_s SNR_0 \left[1 + \sqrt{1 + \frac{v}{a^2}}\right]. \tag{13}$$

If only the idler is selected after point D, we have $\alpha = 0$, and the sensitivity for this case is

$$S(0, \beta) = 2\tilde{P}_s SNR_0 \left[1 + \sqrt{1 + \frac{v}{\beta^2}}\right]. \tag{14}$$

The sensitivity enhancement with single-band FOPA, i.e. with amplified signal (ρ_s) or idler (ρ_i) only after FOPA, over no FOPA case can be quantified by calculating the following ratios respectively,

$$\rho_s = \frac{S(\alpha, 0)}{S_N(\alpha, 0)} = \frac{1 + \sqrt{1 + \frac{v}{\alpha^2}}}{1 + \sqrt{1 + \frac{v_N}{\alpha^2}}} = \frac{1 + \sqrt{1 + \frac{v}{\alpha^2}}}{1 + \sqrt{1 + \frac{v}{\alpha^2} G^2}}, \tag{15}$$

$$\rho_i = \frac{S(0, \beta)}{S_N(\alpha, 0)} = \frac{1 + \sqrt{1 + \frac{v}{\beta^2}}}{1 + \sqrt{1 + \frac{v_N}{\alpha^2}}} = \frac{1 + \sqrt{1 + \frac{v}{\beta^2}}}{1 + \sqrt{1 + \frac{v}{\alpha^2} G^2}}. \tag{16}$$

While the sensitivity enhancement with dual-band FOPA and then single-band FOPA can be determined by the following ratio,

$$\rho_{duals} = \frac{S(\alpha, \beta)}{S(\alpha, 0)} = \frac{1 + \sqrt{1 + \frac{v}{(\alpha + \beta)^2}}}{1 + \sqrt{1 + \frac{v}{\alpha^2}}}, \tag{17}$$

Optics EXPRESS

$$\rho_{duali} = \frac{S(\alpha,\beta)}{S(0,\beta)} = \frac{1+\sqrt{1+\dfrac{v}{(\alpha+\beta)^2}}}{1+\sqrt{1+\dfrac{v}{\beta^2}}}. \tag{18}$$

where ρ_{duals} is the sensitivity ratio of dual-band to signal band only and ρ_{duali} is the ratio of dual-band to idler band only. Based on the above derivations, we can now examine the sensitivity enhancement capability by single-band and dual-band FOPA at different dominate noise situations.

For single-band FOPA, when amplified quantum noise (amplified vacuum fluctuations) dominates over current noise, i.e. $G^2\tilde{P}_s >> \delta i_n^2$, then $v<<1$ is valid. Therefore, the approximations that $\rho_s \approx 1$ and $\rho_i \approx 1$ can be obtained. Since the ratio nearly equals to 1, hence there is no significant sensitivity improvement can be achieved by setting a single-band FOPA before an optical receiver. However, when current noise dominates, i.e. $G^2\tilde{P}_s << \delta i_n^2$, $v>>1$ is valid, and the approximations that $\rho_s \approx 1/G$ and $\rho_i \approx \alpha/(\beta G)$ are obtained. At this situation, $\rho_s < 1$ and $\rho_i < 1$ (by controlling the transmittances ratio of the two paths), which means the sensitivity can be enhanced. For the amplified signal band, the sensitivity enhancement is determined by FOPA gain and the higher gain has higher sensitivity. For the idler band, the sensitivity enhancement is related to the FOPA gain and the transmission loss between signal and idler.

For dual-band FOPA, when amplified quantum noise dominates over current noise, the approximations that $\rho_{duals} \approx 1$, and $\rho_{duali} \approx 1$ are valid since $v<<1$, which means that there is no advantage on sensitivity enhancement as in single-band case. Nevertheless, when current noise dominates, $\rho_{duals} \approx \alpha/(\alpha+\beta)$ and $\rho_{duali} \approx \beta/(\alpha+\beta)$ are available because of $v>>1$. Since $\rho_{duals} < 1$ and $\rho_{duali} < 1$ are always satisfied, dual-band FOPA can further improve the sensitivity than single-band FOPA, and the transmittance ratio determines the final improvement value. The maximum sensitivity enhancement capability by dual-band FOPA is ideally 3-dB larger than that by single-band FOPA when $\alpha = \beta$, i.e. $\alpha/(\alpha+\beta) = \beta/(\alpha+\beta) = 1/2$.

Based on the above qualitative analysis, significant sensitivity enhancement by single- and dual-band FOPA can be achieved when receiver current noise dominates over amplified quantum noise. This condition will be satisfied when the FOPA gain is not too large because the receiver is limited by current noise in low-gain regime, but the beat noise between signal/idler and quantum noise and the beat noise between quantum noise and quantum noise will dominate when the FOPA gain becomes large [45]. Moreover, the ratio of the transmittances of the paths from A to E should be controlled as well to achieve the highest optical receiver sensitivity enhancement capability by FOPA. Both of the gain and transmittances controlling are easy to realize experimentally.

3. Experimental results

3.1 Sensitivity enhancement by single- and dual-band FOPA for WDM communication system

To test the theoretical analysis in WDM communication systems, the SNR_{out} at section 2 corresponds to the required SNR after the receiver to obtain a certain BER, say BER = 10^{-9}, and the sensitivity enhancement by single- and dual-band FOPA can be quantified as the reduction of required minimum power for the certain BER.

In our previous demonstration, a 10-Gb/s return-to-zero on–off keying (RZ-OOK) format WDM system with four WDM channels (wavelength starts from 1545.3nm to 1547.8 nm with 100-GHz spacing) were constructed for this target [18,19]. The receiver sensitivity at BER = 10^{-9} achieved –35.6 dBm, –37.8 dBm, –38.5 dBm, and –38.9 dBm respectively at single-

Optics EXPRESS

band FOPA case (with amplified signal) and the single-band FOPA gain for each channel were 33 dB, 35 dB, 37 dB, and 37 dB. The sensitivity difference between each channel was due to the gain difference experienced by each channel and the transmission loss for the WDM channels was 9 dB. Comparing with channel 1, the FOPA gain of channel 2 ~4 were 2 dB, 4 dB, and 4 dB higher respectively while the sensitivity of channel 2 ~4 were 2.2 dB, 2.9 dB, and 3.3 dB higher than channel 1. These data show that the higher FOPA gain leads to higher detection sensitivity which echoes well with the theory prediction at single-band configuration. At dual-band FOPA case (with amplified signal and idler), the sensitivities were −39.5 dBm, −41.1 dBm, −41.5 dBm, and −42 dBm for each channel, i.e. 3.9 dB, 3.3 dB, 3 dB, and 3.1 dB higher than single-band counterparts, and the transmission loss for the idler band is 7.2 dB. Here, the 1.8 dB transmission loss difference between signal and idler band indicates that the idler have higher sensitivity, and it was this transmission loss difference that caused the measured more than 3-dB sensitivity enhancement at dual-band configuration over single-band case. All the measured data are listed in Table 1.

Table 1. Sensitivity enhancement by FOPA at WDM communication system [19]

WDM channel	Wavelength (nm)	FOPA gain (dB)	Gain difference against channel 1	Sensitivity at BER = 10^{-9}		Sensitivity enhancement	
				Single-band (dBm)	Dual-band (dBm)	Single-band with different gain (dB)	Dual-band against single-band (dB)
1	1545.3	33	–	−35.6	−39.5	–	3.9
2	1546.1	35	2	−37.8	−41.1	2.2	3.3
3	1546.9	37	4	−38.5	−41.5	2.9	3
4	1547.8	37	4	−38.9	−42	3.3	3.1

3.2 Sensitivity enhancement by single- and dual-band FOPA for SS-OCT

In addition to testing at optical communication system, this sensitivity enhancement scheme was also applied in an optical bio-medical imaging modality, i.e. SS-OCT, to improve detection sensitivity and thus to improve the imaging depth. Different from the sensitivity (in dBm) that represents the minimum power for a certain BER in optical communication system, the sensitivity (in dB) in SS-OCT generally represents the dynamic range of the reflected power from bio-sample [46]. Higher sensitivity OCT system supports a larger dynamic range, and thereby paves the way for deeper structure imaging (larger penetration depth).

A SS-OCT based on a Fourier domain mode-locking (FDML) laser served as a typical platform for this purpose and a mud-fish eye was imaged. The optical spectrum bandwidth for OCT was 76 nm. The experimental details are shown in our previous work at [30]. In this experiment, the small interference signal generated by the reflected light from the mud-fish eye and the reference mirror was amplified by a FOPA before it was detected by a receiver. If no FOPA was used, the sensitivity was 72.6 dB, while the imaging depth was ~0.5 mm with 6.3 dBm power on the bio-sample and the interference signal's power was −42 dBm. At this case, only the surface of cornea and iris could be observed as shown in Fig. 2(a). However, when the detection sensitivity was enhanced by a single band-FOPA, the sensitivity was improved to 82.4 dB with 10.5 dB average FOPA gain for the 76-nm optical spectrum bandwidth. Although the imaging depth has no obvious improvement, the lens surface and the gap between the lens and cornea were clearly shown at the same illumination power level, as is shown in Fig. 2(b). Furthermore, when dual-band FOPA was used, the sensitivity was improved to 84.8 dB, while the imaging depth achieved to ~1.7 mm and even the retina structure was exhibited, as is shown in Fig. 2(c). In this experiment, the sensitivity improvement by a single-band FOPA (with amplified signal band) was 9.8 dB while it was

Optics EXPRESS

12.2 dB at dual-band configuration, i.e. 2.4 dB higher than single-band FOPA. Those experiment results match well with the theory counterparts at section 2.

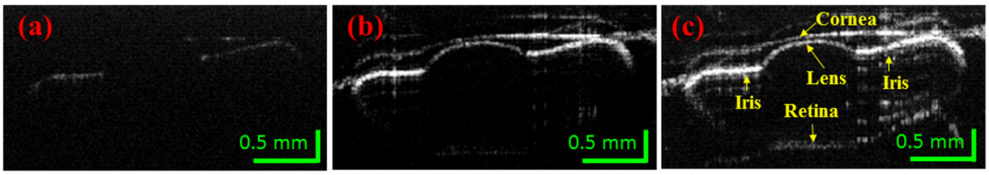

Fig. 2. SS-OCT images at different cases [30]. (a): conventional image; (b): image with single-band FOPA; (c): image with dual-band FOPA.

It is noted that quantum theory could be used to give a rigorous description on the two-mode squeezing process of FOPA and noise fluctuations, and the proposed semi-classical model would not reveal the underlying physics of FOPA as profound as those models based on quantum theory. However, comparing with quantum analysis, semi-classical model would still capture the essence of the receiver sensitivity enhancement scheme by FOPA through our experimental results. We have not identified any obvious mismatch between the theoretical analysis and experimental results as is discussed at this section. This model provides an essential understanding without probing further into quantum mechanics as it focuses on the basic principles of sensitivity enhancement by using single- and dual-band FOPA.

4. Conclusions

In this paper, a theoretical analysis based on semi-classical model is elaborated for the working principles of an optical receiver sensitivity enhancement scheme through single- and dual-band FOPA. The sensitivity enhancement by single-band FOPA is determined by FOPA gain and transmittance of signal and idler, and the sensitivity can be further improved by 3-dB through using signal and idler together at dual-band configuration. The validation of the theoretical analysis are broadly examined on optical fiber communication system and optical bio-medical imaging modality, and those experimental results match well with the theoretical counterparts. This detection sensitivity enhancement scheme can be potentially applied in the scenarios where ultrafast broadband signal at low-power level is being handled, such as in fiber communication system and biomedical imaging area.

Funding

Research Grants Council of the Hong Kong Special Administrative Region, China (Project Nos. E-HKU701/17, HKU 17205215, HKU 17208414, and CityU T42-103/16-N) and National Natural Science Foundation of China (N_HKU712/16). Innovation and Technology Fund (GHP/050/14GD); and University Development Fund of HKU.

Acknowledgments

In memory of Professor Michel E. Marhic, a pioneer in the research of fiber optical parametric amplifiers, who was deceased unexpectedly in August 2014.